Influence of Visual-Inertial Sensor-To-Segment Calibration on Upper Limb Joint Angles Estimation from Multiple Inverse Kinematics Methods

Mohamed Adjel, Raphael Dumas, Samer Mohammed, Vincent Bonnet

Influence of Visual-Inertial Sensor-To-Segment Calibration on Upper Limb Joint Angles Estimation from Multiple Inverse Kinematics Methods

Mohamed Adjel[1,2], Raphael Dumas[3], Samer Mohammed[2], Vincent Bonnet[4, 5]

***Abstract*—This study aims to explore the potential for accurately estimating joint angles during upper limb rehabilitation tasks with different calibration procedures, inverse kinematics methods and measurement modalities. Affordable embedded visual-inertial measurement units offer a promising alternative to the costly and cumbersome gold standard marker-based optical motion capture systems. However, affordability comes with inherent sensors inaccuracies. Hence, prior to their application in a real clinical setting, it is important to demonstrate their ability for accurate joint angle estimation. Discrepancies in joint angles arise due to the inaccuracies of different sensing modalities but also to sensor-to-segment calibration procedures that significantly alter the joint offsets. Therefore, in this paper, the impact of functional and anatomical calibration procedures on joint angle estimation was compared among seven healthy young volunteers. When the same calibration procedures were applied with visual-inertial measurement units and optical motion capture systems data, a relatively small root mean square error of 7.9 deg and correlation coefficients exceeding 0.86 were observed. When different calibration procedures were applied with visual-inertial measurement units and optical motion capture systems data, higher root mean square superior to 10 deg were observed, highlighting the importance of consistency with the reference set when assessing accuracy. Furthermore, our analysis shows the benefit of using multi-body inverse kinematics procedure over treating inverse kinematics separately for each segment when dealing with inaccurate visual-inertial measurement units data.**

***Note to Practitioners*—This study addresses the practical challenge of accurately estimating upper limb joint angles in rehabilitation, using affordable Visual-Inertial Measurement Units (VIMUs) and cameras. The key finding for practitioners is the importance of consistent calibration procedures, either anatomical or functional, across both VIMUs and standard reference systems. This consistency significantly improves measurement accuracy, essential for effective rehabilitation assessment and planning. We also demonstrate that multi-body inverse kinematics (IK) methods are more reliable than single-body IK when using data from low-cost sensors. Multi-body IK better handles inaccuracies typical of affordable devices, making it a more suitable choice for clinical applications. While our results are promising, they are based on controlled conditions and do not encompass whole-body movements. Future research should focus on extending these findings to more diverse and challenging clinical scenarios, ensuring the practical applicability of this cost-effective technology in real-world rehabilitation settings.**

***Index Terms*—Inverse kinematics, Affordable Visual-inertial Measurement Units, Human Model Calibration.**

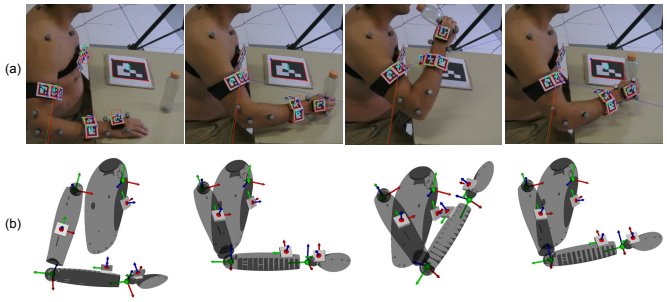

Fig. 1: (a) successive snapshots of different postures during bottle task, and (b) the corresponding reconstructed 3D joints kinematics estimated with multi-body IK and Visual-Inertial Measurement Units.

I. Introduction

Upper limbs functional impairments among post-stroke patients affect their ability to accomplish daily life activities. Rehabilitation exercises monitored by clinicians, like the Frenchay Arm Test (FAT) [1], enhance limb mobility and overall quality of life. However, visually assessing complex motions during rehabilitation introduces inter/intra-clinician variability in the evaluation of limbs mobility [2]. Clinical indices used to monitor limb mobility and rehabilitation progress depend on the accurate estimation of joint angles, which are obtained through Inverse Kinematics (IK), a process that retrieves joint angles from Cartesian measurements. Using measured Cartesian data, joint angles can be determined through either a single-body IK or a multi-body IK approach. Single-body IK estimates the joint angles directly from each segment/sensor rotation and/or position. On the other hand, multi-body IK simultaneously determines the pose of all segments while considering constraints imposed by different joints [3], [4], making it more resilient to soft-tissue artifacts and measurement outliers [5], [6]. Multi-body IK is more robust to measurement outliers in Cartesian data from affordable sensors due to fixed segment lengths and joint limits [3], [5]–[7].

[1]NaturalPad, 70 ancien chemin de Saint-Vincent, Montpellier, France
[2]LISSI, Domaine Chérioux, 122 rue Paul Armangot, Vitry-sur-Seine, France
[3]Univ Lyon, Univ Gustave Eiffel, Univ Claude Bernard Lyon 1, LBMC UMR T_9406, Lyon 69622, France
[4]LAAS-CNRS, 7 avenue du Colonel Roche, Toulouse 31031, France
[5]Image and Pervasive Access Laboratory (IPAL), CNRS-UMI, 2955, Singapore.

Gold-standard Optical Motion Capture (OMC) systems provide accurate Cartesian data, but are limited in real-world use due to cost and portability constraints, making them more suitable for laboratory settings. To overcome these limitations, studies propose alternatives like cost-effective sensors using RGB, RGB-Depth, and markerless algorithms [8]–[10], Inertial Measurement Units (IMU) [11], IMU with RGB-D data fusion [12], [13], or IMU and fiducial markers fusion using Visual-Inertial Measurement Units (VIMU) [7], [14].

However, inaccurate input data and poorly calibrated kinematic models can lead to Root Mean Square Error (RMSE) exceeding 20 deg, when comparing joint angles from markerless data with joint angles obtained from OMC data [15]. Markerless data, besides providing unrealistic joint center estimates, lacks access to essential anatomical landmarks for biomechanical model definition, leading to significant calibration offset errors compared to OMC [16]. However, recent research [17] demonstrated the possibility of using machine learning to train a neural network inferring anatomical landmarks positions from markerless data, with an average accuracy of 15.2 mm for upper limbs anatomical landmarks. Despite outstandingly promising results for the considered set of 10 participants [17], the method has not yet demonstrated its capability to accurately estimate anatomical landmarks positions on large scale datasets with movements different from the ones in its training set. Furthermore, markerless approaches suffer from occlusions, and several studies proposed to use wearable sensors such as IMUs and VIMUs to compensate for the occlusions in 3D joints kinematics estimation [18]–[21].

When using wearable sensors, sensor-to-segment calibration procedures are crucial in achieving accurate estimates of 3D joints kinematics. In the literature four calibration procedures were proposed:

- static calibration, which relies on predetermined limb anatomical poses [22], [23],
- technical calibration that assume alignment between sensor technical axes and segment anatomical axes [22], [24],
- functional calibration, in which the subject is instructed to perform specific joint-by-joint motion [14], [25],
- anatomical calibration [18], [26]–[28], where anatomical landmarks are pinpointed onto the subject.

Static and technical calibration methods, though user-friendly, rely on the subject's ability or clinician's skill, leading to misalignment and inaccurate joint angles estimates [22], [23], mainly due to large joint axis offsets [16]. Notably, the anatomical approach, recommended by the International Society of Biomechanics [26], is commonly advised. However, the practical choice of calibration procedures for affordable sensors, like IMUs, remains unclear, despite their widespread use and availability in commercial products, which often employ static calibration procedures. Recent approaches [21], [29] proposed to use large datasets [30]–[33] of diverse human movements to train neural networks estimating 3D joints kinematics. Shin et al. [21] obtained promising results in 3D joints kinematics estimation and even proposed a method that does not require sensor-to-segment calibration. However, the datasets used for the training of neural networks relied on ground-truth marker-sets different from the ones recommended by the International Society of Biomechanics [26], which could lead to large differences between the ground-truth assumed by these datasets and the real joint angles. When evaluating the accuracy of their methods, the studies using machine learning approaches [21], [29] relying on these datasets do not investigate this issue, and do not validate the accuracy of their methods on datasets using marker-sets recommended by the International Society of Biomechanics.

Estimating IMUs' positions with respect to the segments frames isn't feasible with anatomical calibration, but their rotation can be estimated [18], [27]. Researchers like Meng et al. [19] suggested using four IMUs and functional calibration [25] to estimate upper arm joint angles, reporting a 5.79 deg RMSE compared to OMC, after removing the calibration offset. They considered a reduced model of the upper limb, omitted a comparison between anatomical and functional calibration, and relied on anthropometric tables for segment lengths. Notably, the abovementionned studies [18], [19], [21], [29], used IMUs relying on magnetometers for rotation estimation. However, this is not recommended for clinical applications due to magnetometers' sensitivity to ferromagnetic disturbances [34].

To avoid the use of magnetometer in a clinical context, several studies proposed to use fiducial markers along with IMUs, in a so-called VIMU, and demonstrated promising accuracy in upper limb model construction and joint angles estimation [7], [14], [20]. Both anatomical [7] and functional calibrations [14] are feasible. Mallat et al. [7] used anatomical calibration and achieved a 2.7 deg RMSE for upper limb joint angles compared to OMC, with the calibration offset removed. Li et al. [14] proposed technical and functional calibration for an upper limb biomechanical model, reporting an excellent 2.3 deg average RMSE compared to OMC joint angles without calibration offset removal. However, both studies did not discuss the comparison of functional and anatomical calibration procedures, the influence on joint angles accuracy when considering different reference sets, and the benefits of using a multi-body IK over single-body IK for joint angles estimation when considering these VIMU measurements.

The main goal of this paper is to evaluate the precision of upper limb joint angle estimations using cost-effective VIMUs priced under 15€ and affordable cameras under 70€. This evaluation encompasses both anatomical and functional sensor-to-segment calibration procedures. The study also explores how accuracy varies with different reference data sets. Additionally, we compare the effectiveness of multi-body versus single-body IK methods when applied to VIMU data. For a visual summary of this comparative analysis, refer to Figure 2, with a detailed explanation provided in Section II-D.

II. Materials and Methods

A. Sensor-to-segment calibration

The sensor-to-segment calibration is a subject-specific calibration procedure that estimates the transformation matrix representing the position and rotation of the VIMU relatively to its corresponding segment frame. This transformation matrix is

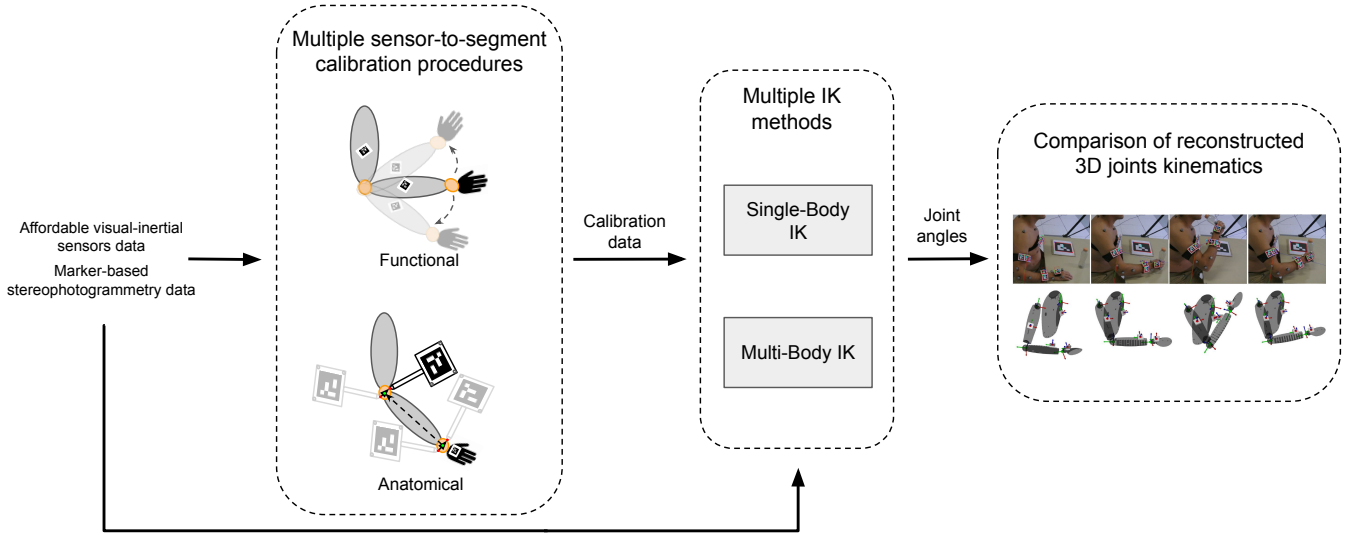

Fig. 2: Overview of the proposed comparative study.

necessary to calculate biomechanically meaningful joint angles for both single-body and multi-body IK. We compared two calibration procedures, namely anatomical and functional, to determine the rigid body transformation between the VIMU and the segment frames.

Anatomical calibration. Utilizing a calibration wand, 11 anatomical landmarks were pinpointed on the participant (see Fig. 5). The anatomical landmarks were: the processus xiphoideus, acromion, incisura jugularis, C7 cervical vertebra, T8 thoracic vertebra, lateral epicondyle, medial epicondyle, radial styloid, ulnar styloid, second metacarpal head, and fifth metacarpal head. The positions of these landmarks in the VIMU's frame were determined to build anatomical frames [26]. Typically, the medio-lateral axis of each segment was determined through the normalized position of two markers (or pin-pointed points) fixed on the segment, the longitudinal axis was determined as the normalized translation vector between parent and child segment, and the antero-posterior axis was determined as the cross product of medio-lateral and longitudinal axes. Those three axes allowed to construct the rotation matrix of the segment, and its origin was coincident with the joint center position of the proximal joint [26] (i.e. wrist for the hand, elbow for the forearm, and shoulder for the upperarm). The trunk frame was positioned at the jugular notch center, the upper arm frame at the gleno-humeral center using the bi-acromial distance ratio [35], the forearm frame at the midpoint between medial and lateral epicondyle, and the hand frame at the midpoint between radial and ulnar styloid.

Functional calibration. Employing the SCoRE method [36] for joint center estimation and the SARA method [37] for determining joint axes, the participant performed specific movements. For wrist joint center and axis estimation, uni-axial wrist flexion/extension movements were executed; for elbow joint center and axis estimation, elbow flexion/extension movements; and for shoulder joint center estimation, shoulder circumduction movements. The consecutive joint centers of rotation were used to define the segment's longitudinal functional axes. Cross products between estimated axes and longitudinal axes were used to reconstruct segment frames centered on the parent joint center of rotation.

B. *Upper limbs biomechanical model*

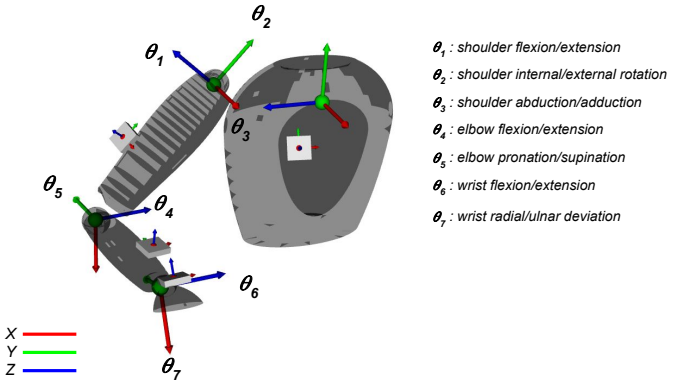

Fig. 3: Biomechanical model frames and degrees of freedom.

VIMU measurements were related with the joint kinematics using a biomechanical model composed of $N_s = 4$ rigid segments articulated with $N_j = 7$ degrees of freedom. The relative rotation of each segment in the kinematic chain, as well as the order of rotations, were defined following the International Society of Biomechanics recommendations [26]. The upper arm segment was linked to the trunk through three revolute joints, the forearm segment was linked to the upper arm through a universal joint (i.e. 2 successive revolute joints), and the hand segment was linked to the forearm through a universal joint. A total of 4 VIMUs were rigidly linked to each segment using their local pose obtained either through anatomical or functional calibration. The model floating base location w.r.t camera frame c was set using three prismatic and three revolute joints. The rotation $\mathbf{R}_v^c$ and position $\mathbf{p}_v^c$ of the VIMU frame v with respect to the camera frame were

calculated using the Forward Kinematics Model (FKM) as follows:

$$[\mathbf{p}_v^c \ \mathbf{R}_v^c] = FKM(\boldsymbol{\theta}, \boldsymbol{\phi}) \tag{1}$$

where $\boldsymbol{\theta}$ is the vector of joint angles and $\boldsymbol{\phi}$ is the vector containing local VIMU poses and segments lengths obtained either through the functional or anatomical calibration procedures. The 3D angular velocities $\boldsymbol{\omega}_v^v$ and linear accelerations $\mathbf{a}_v^v$ of the VIMU w.r.t its own frame were estimated with the first and second differential models, respectively:

$$\begin{aligned} \boldsymbol{\omega}_v^v &= \mathbf{R}_v^{c^T} \mathbf{J}_r \dot{\boldsymbol{\theta}} + \mathbf{b}_\omega \\ \mathbf{a}_v^v &= \mathbf{R}_v^{c^T} (\mathbf{J}_p \ddot{\boldsymbol{\theta}} + \dot{\mathbf{J}}_p \dot{\boldsymbol{\theta}}) + \mathbf{b}_a \end{aligned} \tag{2}$$

where $\dot{\boldsymbol{\theta}}$ and $\ddot{\boldsymbol{\theta}}$ are the joint velocity and acceleration vectors, respectively. $\mathbf{b}_a$ is the acceleration bias and $\mathbf{b}_\omega$ the gyroscope bias. $\mathbf{J}_p$ and $\mathbf{J}_r$ are the position and rotation Jacobian matrices expressed in the camera frame, respectively. The estimated measurement vector $\mathbf{h}$ was then defined as follows:

$$\mathbf{h} = [\mathbf{p}_v^c \ \mathbf{q}_v^c \ \mathbf{a}_v^v \ \boldsymbol{\omega}_v^v] \tag{3}$$

where $\mathbf{q}_v^c$ is the quaternion that corresponds to the 3D rotation matrix $\mathbf{R}_v^c$, provided from aruco library [38], [39]. Pinocchio library [40], that efficiently implements state-of-the-art rigid body algorithms for poly-articulated systems, was used to calculate the FKM and its derivatives.

C. Inverse kinematics

In this study, we compared two Extended Kalman Filter (EKF)-based IK methods for joint angle estimation. The first multi-body IK approach relied on a biomechanical model of the upper limbs whereas the second, which was a single-body IK, used solely 3D measurements of each VIMU sensors separately to estimate joint angles.

Multi-body inverse kinematics. The EKF corresponding to the multi-body IK estimates a state vector $\mathbf{x}_k = \left[\boldsymbol{\theta} \ \dot{\boldsymbol{\theta}} \ \ddot{\boldsymbol{\theta}} \ \mathbf{b}_a \ \mathbf{b}_\omega\right]$ that minimizes, at each sample k, the least squares difference between the measurement vector $\mathbf{y}_k$ and its corresponding estimated vector $\mathbf{h}_k$. The measurement vector $\mathbf{y}_k = [\mathbf{p}_v^c, \ \mathbf{q}_v^c, \ \mathbf{a}_v^v, \ \boldsymbol{\omega}_v^v]$ consists of the measured 3D positions, rotations, angular velocities, and linear accelerations of the VIMU. The process and measurement models were modeled as follows:

$$\begin{aligned} \mathbf{x}_{k+1} &= f(\mathbf{x}_k) + \mathbf{w}_k \\ \mathbf{h}_k &= h(\mathbf{x}_k) + \mathbf{v}_k \end{aligned} \tag{4}$$

where f denotes the state process model, assuming that the joint positions and velocities are evolving linearly while accelerations and biases remain constant [41]. h is the measurement model that maps a measurement vector $\mathbf{h}$ to a state vector $\mathbf{x}_k$ through the FKM (1), and the first and second order differential models (2). $\mathbf{w}_k$ and $\mathbf{v}_k$ represent the process and measurement noise, respectively.

The update of the state vector is determined as follows:

$$\begin{aligned} \boldsymbol{\epsilon}_k &= \mathbf{y}_k - h(\mathbf{x}_{k|k-1}) \\ \mathbf{x}_{k|k} &= \mathbf{x}_{k|k-1} + \mathbf{K}_k \boldsymbol{\epsilon}_k \end{aligned} \tag{5}$$

where $\mathbf{x}_{k|k-1}$ is the state predicted from $\mathbf{x}_{k-1}$ through the process model, and $\mathbf{x}_{k|k}$ is the updated state. $\mathbf{K}$ is the Kalman gain and $\boldsymbol{\epsilon}_k$ is the error between VIMUs measurements and predicted measurements. To ensure the EKF stability and convergence, it's essential to finely tune the covariance matrices of the process noise $\mathbf{w}_k$ and the measurement noise $\mathbf{v}_k$, as well as the the initial state $\mathbf{x}_0$ and its covariance. $\mathbf{x}_0$ was estimated using an inverse geometric model optimized as per Lu et al. [3], which consists in determining the joint angles that minimize, in a least squares sense, the difference between measured VIMUs positions/rotations, and the ones estimated from the joint angles processed through the FKM (1). Consequently, its covariance was initialized as an identity matrix, implying high confidence uniformly across all states. The measurement noise covariance was derived from the average difference between reference (OMC data) and sensor (VIMU data) measurements, using specific trials that were excluded from the results section. Process noise covariance matrix tuning was influenced by employing a constant acceleration model, which does not represent well human motion due to its non-constant joint accelerations. This discrepancy becomes more pronounced in high-speed movements. Nevertheless, in the context of rehabilitation, where motions are typically slower, the impact is less severe. To accommodate this, covariances for joint velocities and accelerations were set to a fixed value of 10^3, a common practice in relevant literature [42], [43]. Conversely, as the process model for joint angles is more accurate, its covariance was assigned a value of 1.

Single-body inverse kinematics. Single body IK calculates the joint angles from the relative rotations of successive segments frames, as the relative rotation of VIMUs would not correspond to biomechanically meaningful joint angles. Thus, the rotation of each body segment was estimated using a single-body IK EKF relying on the VIMU rotation measurement, expressed as a quaternion, and the rigid transformation matrix between the VIMU and its corresponding segment, which was obtained during the sensor-to-segment calibration phase.

The state vector $\mathbf{x}_k = [\mathbf{q}_s^c, \ \mathbf{b}_\omega]$ consists of the rotation of the segment frame s relative to the camera frame, expressed as a quaternion $\mathbf{q}_s^c$ and the gyroscope bias, denoted as $\mathbf{b}_\omega$. The prediction of the state was made using the angular velocity of the segment $\boldsymbol{\omega}_s^c$ [44]:

$$\dot{\mathbf{q}}_s^c = \frac{1}{2} \Omega(\mathbf{q}_s^c) \boldsymbol{\omega}_s^c, \tag{6}$$

$$\text{with } \Omega(\mathbf{q}_s^c) = \begin{bmatrix} -q_1 & -q_2 & -q_3 \\ q_0 & -q_3 & q_2 \\ q_3 & q_0 & -q_1 \\ -q_2 & q_1 & q_0 \end{bmatrix}, \tag{7}$$

$$\text{and } \boldsymbol{\omega}_s^c = \mathbf{R}_s^c \mathbf{R}_v^s \boldsymbol{\omega}_v^v, \tag{8}$$

with $\mathbf{R}_v^s$ the VIMU rotation w.r.t the segment frame, obtained either through anatomical or functional calibration. The process model was expressed as follows:

$$\mathbf{x}_{k+1} = \begin{bmatrix} \mathbf{I}_{4\times4} & -\frac{\Delta t}{2}\Omega(\mathbf{q}^c_{s_k}) \\ \mathbf{0}_{3\times4} & \mathbf{I}_{3\times3} \end{bmatrix} \mathbf{x}_k + \begin{bmatrix} \frac{\Delta t}{2}\Omega(\mathbf{q}^c_{s_k}) \\ \mathbf{0}_{3\times3} \end{bmatrix} \boldsymbol{\omega}^c_{s_k} + \mathbf{w}_k \tag{9}$$

The measurement vector $\mathbf{y}_k$ includes the quaternion $\mathbf{q}^c_{v_k}$, which represents the rotation of the VIMU in the camera frame. The measurement model h is thus expressed as:

$$h(\mathbf{q}^c_{s_k}) = \mathbf{q}^c_{s_k} \otimes \mathbf{q}^s_v \tag{10}$$

where $\otimes$ denotes the operator for quaternion multiplication and $\mathbf{q}^s_v$ represents the rotation of the VIMU in the local segment frame, which is determined using either the anatomical or functional calibration procedure. The equations of the update step are identical to those represented in Eq. (5). The covariance matrices of the process model and measurement model noises were derived from the average difference between reference (OMC data) and sensor (VIMU data) measurements, using specific trials that were excluded from the results section.

D. Comparative analysis

We compared joint angle estimates across various conditions: using OMC and VIMU measurements, anatomical and functional calibration procedures, and multi-body versus single-body IK methods. In multi-body IK, both calibration procedures involved estimating segment lengths and retro-reflective markers/VIMU position/pose in their segment frames, defining joint angles as rotations around the axes defined in the biomechanical model (see Section II-B). For single-body IK both calibrations focused solely on determining the rotation of retro-reflective markers/VIMU technical frames in their segment frames. Relative segment rotations produced the attitude vector [45], that was projected onto anatomical/functional axes of the parent segment to calculate rotation angles [46]. This approach avoids gimbal lock issues while providing an easily interpretable alternative to Euler angles. Four sets of reference joint angles were determined using the 3D positions of retro-reflective markers. Two of these sets were derived using single-body IK, as referenced in [46], and were calibrated either anatomically or functionally. The two additional sets were derived from the model presented in Section II-B and relied on a classical multi-body IK approach [47]. This approach involved an EKF in combination with a FKM to estimate reference joint angles. These angles were computed to reproduce marker positions (using the FKM) that best matched those measured by the OMC. The FKM depended on calibration parameters obtained through either anatomical or functional calibration methods. An EKF was used for these sets to ensure algorithmic consistency between IK based on VIMU data and IK based on OMC data. To further ensure consistency and account for the differences between single-body and multi-body IK methodologies, we conducted specific comparative analyses. Joint angles derived from VIMU using single-body IK were compared exclusively with those obtained from OMC data via single-body IK.

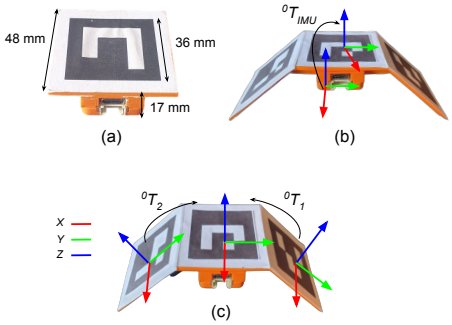

Fig. 4: 3D-printed VIMUs, equipped with a ESP32-PICO microcontroller, costing 15€. (a) Dimensions of the VIMU, (b) transformation matrix from IMU frame to fiducial marker frame, (c) transformation matrices between fiducial markers frames. The angles of the VIMU wings were chosen to minimize occlusion occurrences and maximize ergonomics.

Similarly, joint angles acquired from VIMU through multi-body IK were compared with corresponding joint angles derived from OMC data using multi-body IK. This allowed for a more accurate and methodologically consistent comparison across the different sets. Furthermore, we also compared joint angles from OMC and VIMU measurements, with and without calibration offset removal. This aspect of the analysis is crucial, as the presence or absence of calibration offsets can substantially impact the results. Segment lengths and local VIMU rotations from anatomical and functional calibrations were compared for their impact on joint angle estimation.

E. Experimental setup

Seven participants (five males, two females, 71.6 ± 16 kg, 27.6 ± 6 years, 1.72 ± 0.1 m) performed one trial of three repetitions of pick and place, ruler, and bottle tasks of the Frenchay Arm Test [1]. These tasks involved placing 11 markers on anatomical landmarks (see Section II-A). Participants gave written informed consent prior to engaging in the experimental procedures. Two affordable rolling-shutter cameras (*ELP-usbfhd08s*, 1920x1080 MJPEG, 30fps, 70€) were positioned in front and on the side of the participant. Intrinsic and extrinsic parameters of both cameras were estimated using 50 static chessboard poses and OpenCV[1]. A calibration wand was designed using a fiducial marker with a length of 0.18m and three reflective markers, as depicted in Fig. 5. Wand tip position was calibrated with a sphere fitting method, resulting in a 0.1 mm residual using reflective markers and 3 mm using the fiducial marker. Using tip positions of both wands, an overdetermined system of equations was solved to estimate the transformation matrix between cameras and OMC base frames [48], with an an average residual of 8.0 ± 0.3 mm. Fig. 1 shows a camera view of a participant during the bottle task and reconstructed joint kinematics.

III. Results

Table I presents a comparison of joint angle estimates obtained from VIMU and OMC data. It specifically compares

[1]https://opencv.org/

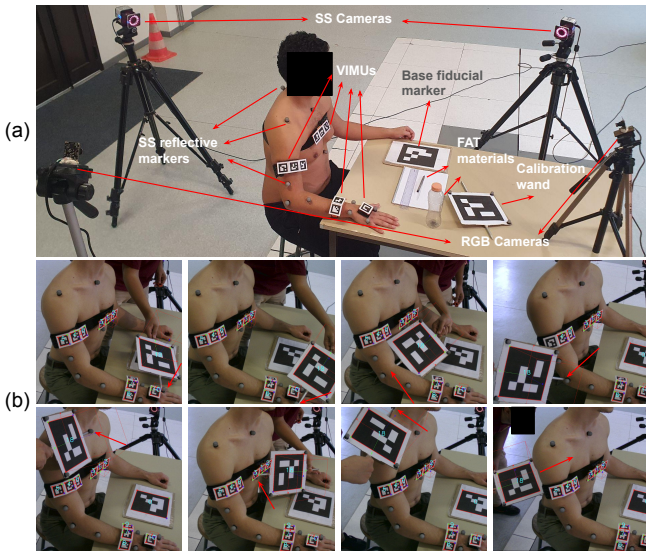

Fig. 5: (a) Experimental setup with marker-based OMC and affordable system based on two affordable cameras and VIMUs. (b) Anatomical calibration process performed with the calibration wand. The base fiducial marker, placed parallel to the ground, was used to determine the gravity vector w.r.t. camera frame c.

these estimates against four reference sets of joint angles, derived from OMC data, as explained in section II-D. The comparison metrics used are the RMSE and the Pearson correlation coefficient (r). When the set of reference joint angles was compared with the joint angles calculated from VIMU data, both based on a multi-body IK and an anatomical calibration procedure, an average RMSE of 9.6 deg and r value of 0.78 were observed. Using functional calibration for VIMU-based multi-body IK slightly increased RMSE to 10.6 deg and an r value of 0.87. Conversely, when joint angles were calculated with functional calibration and multi-body IK for both OMC and VIMU data, an average RMSE of 7.9 deg and an r value of 0.87 were observed. However, using anatomical calibration for multi-body IK with VIMU data resulted in an average RMSE of 10.9 deg and an r value of 0.78.

Interestingly, reporting joint angles by removing average calibration joint offsets, a common practice in the literature [7], [16], [19], reduced the mentioned RMSE to 2.7 deg, 2.7 deg, 2.3 deg, and 2.4 deg, respectively. Table I also highlights that multi-body IK consistently reduces RMSE and increases r in all comparisons. The RMSE with single-body IK consistently exceeded multi-body IK RMSE when comparing joint angles from both OMC and VIMU data. Even after removing the joint offset calibration, the RMSE remained twice as high with single-body IK compared to multi-body IK.

Finally, the functional and anatomical calibration comparison, using only OMC data, reveals joint angles are very close when the calibration offset is removed, with an average RMSE below 1 deg and a high r value of 0.99. However, when the calibration offset was not removed, differences of 5 deg were observed between both reference sets.

Table II shows a comparison of the model segment lengths obtained from anatomical and functional calibration procedures using OMC or VIMU data. When using the same calibration procedure, regardless of the measurement type, the segment lengths were notably similar, showing an average difference of 2 mm. However when comparing anatomical and functional calibration procedures, the average difference was of 30 mm or about 10% of the total segment length.

Table III describes the average local VIMU' 3D rotation, expressed as ZYX Euler angles, in their respective segment frames. As depicted in Fig. 3 the Z, Y and X axes represent the rotations in the medio-lateral, the cranio-caudal and antero-posterior planes, respectively. The average rotation along the Z and X axes was relatively low for all segments. On the other hand, for the Y axis, it was notably larger, measuring 12 deg when anatomical calibration was applied and 11.7 deg with functional calibration. The largest angle was observed for the VIMU attached to the upper arm that was due to the adapted VIMU placement on the upper arm for participants' morphological differences. Across all segments, one can see that the anatomical and functional calibration yield relatively different local VIMU pose. This disparity, is discussed in next section.

IV. Discussion

When comparing joint angles estimated from VIMU with those estimated from a reference OMC, the two main sources of error are the inaccuracy of VIMU measurements tracked during the IK and the calibration offsets. VIMU measurements tracked during the IK process contain intrinsic noise and inaccuracies compared to reference measurements. On the other hand, the calibration offset is caused by measurement inaccuracies during the calibration phase and/or by the difference in rotation of joints axis of rotation intrinsic to each calibration procedure.

When the same calibration procedure is used for OMC and VIMU IK, the calibration offset results solely from measurement inaccuracies during the calibration process. In the case of anatomical calibration, the offset is due to inaccuracies in VIMU pose estimation, to differences between the wand's local tip positions, and to differences between the wand's pose estimated from fiducial marker and reflective markers. In the case of functional calibration, the offset is due to inaccuracies in the estimated VIMU poses during calibration motions. When different calibration procedures are used to compare joint angles estimated from VIMU and OMC, an additional offset arises due to the distinction between anatomically defined joint axes of rotation, based on anatomical landmarks, and functionally defined joint axes of rotation, established through motion.

The smallest RMSE (7.9 deg) is achieved when comparing joint angles calculated from VIMU functional calibration with reference joint angles calculated from functional calibration. The anatomical calibration procedure, relying on anatomical landmarks with one 3D position measurement per landmark, contrasts with the functional calibration procedure, which utilizes motion measurements and least squares minimization

TABLE I: Average accuracy of joint angles obtained from different sensing modalities, IK methods and calibration methods. The metrics considered are the average RMSE, RMSE with calibration offset removed and Pearson correlation coefficient (r). For details about the comparative analysis, refer to section II-D.

-	RMSE [deg]		RMSE offset removal [deg]		r	
	OMC anatomical	OMC functional	OMC anatomical	OMC functional	OMC anatomical	OMC functional
VIMU multi-body IK anatomical	9.6 $\pm$ 3.2	10.9 $\pm$ 2.9	2.7 $\pm$ 1.1	2.4 $\pm$ 0.9	0.78 $\pm$ 0.1	0.79 $\pm$ 0.1
VIMU multi-body IK functional	10.6 $\pm$ 2.7	7.9 $\pm$ 2.3	2.7 $\pm$ 1.2	2.3 $\pm$ 0.8	0.87 $\pm$ 0.1	0.87 $\pm$ 0.1
VIMU single-body IK anatomical	14.1 $\pm$ 4.3	14.1 $\pm$ 4.5	4.8 $\pm$ 2.7	4.6 $\pm$ 2.9	0.57 $\pm$ 0.2	0.63 $\pm$ 0.2
VIMU single-body IK functional	14.0 $\pm$ 4.1	12.1 $\pm$ 4.3	5.5 $\pm$ 2.2	4.9 $\pm$ 2.4	0.56 $\pm$ 0.2	0.68 $\pm$ 0.2
OMC multi-body IK anatomical	-	5.1 $\pm$ 0.7	-	0.8 $\pm$ 0.1	-	0.99 $\pm$ 0.0
OMC multi-body IK functional	5.1 $\pm$ 0.7	-	0.8 $\pm$ 0.1	-	0.99 $\pm$ 0.0	-

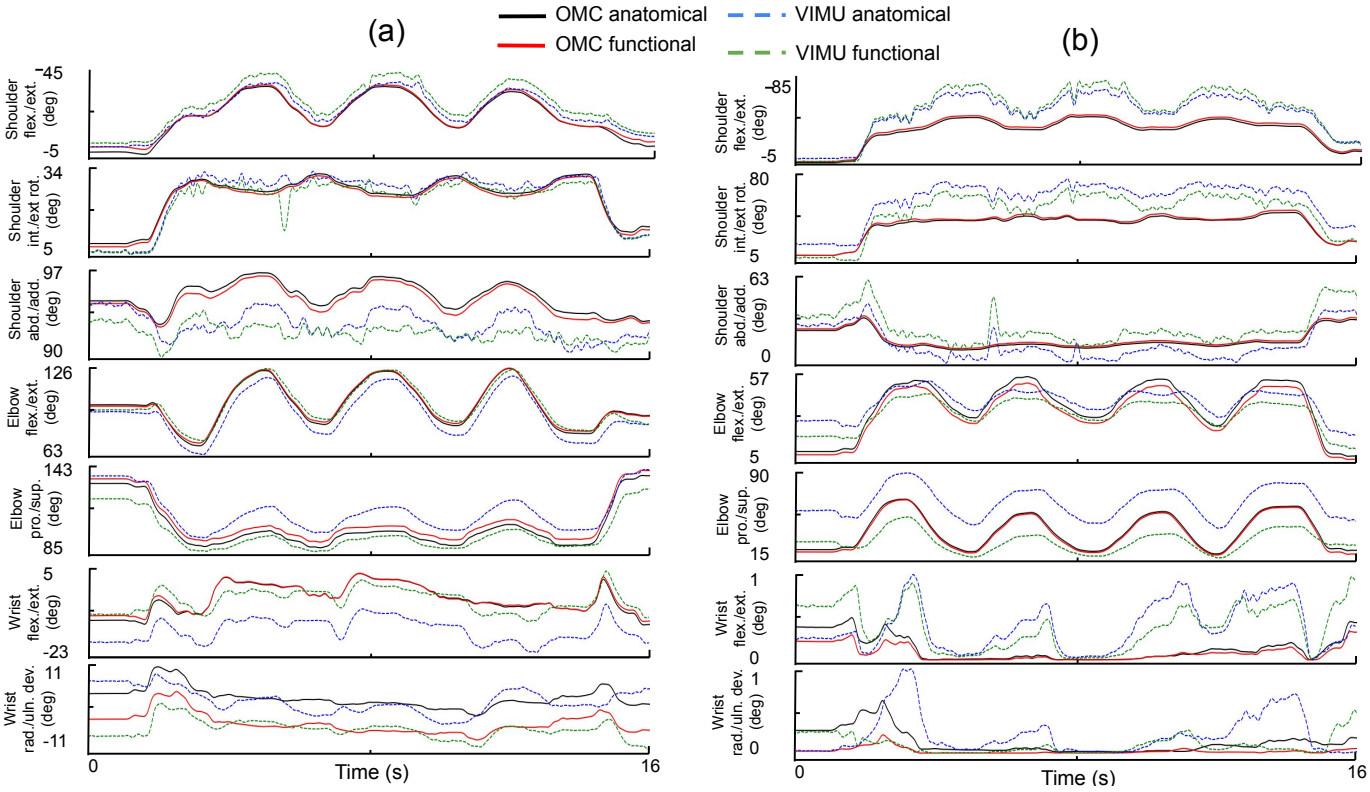

Fig. 6: Upper limbs joint angles estimated during a typical bottle task, using multi-body (a) and single-body (b) IK methods, from OMC data with anatomical calibration (black), from OMC data with functional calibration (red), from VIMU data with anatomical calibration (dashed blue) and from VIMU data with functional calibration (dashed green).

TABLE II: Upper limbs segments lengths estimated OMC and VIMU data through both anatomical and functional calibration procedures.

-	Upper arm length [m]	Forearm length [m]
OMC anatomical	0.279 $\pm$ 0.01	0.259 $\pm$ 0.01
OMC functional	0.310 $\pm$ 0.02	0.256 $\pm$ 0.01
VIMU anatomical	0.281 $\pm$ 0.01	0.258 $\pm$ 0.01
VIMU functional	0.320 $\pm$ 0.01	0.256 $\pm$ 0.02

[49], [50], suggesting the latter's robustness. Nonetheless, the RMSE of 7.9 deg when using functional calibration procedure remains higher than the one obtained by Li et al. [14] that used the same method. This difference can be attributed to two key factors in their study: first, they employed a simplified upper limb model that accounted for only 4 degrees of freedom, compared to the 7 degrees of freedom considered in our study. Secondly, Li et al. used larger fiducial markers than the 36 mm ones in our setup (see Fig. 4). While larger markers enhance pose estimation accuracy, they also add to the system's bulkiness.

Table II reveals segment length variations between anatomical and functional calibration. The upper arm's significant variation is attributed to different definitions of the shoulder center between anatomical [35] and functional [49] calibration procedures. Notably, the difference in upper arm length obtained with VIMU and OMC using anatomical calibration is only 2 mm. Accurate forearm length estimation is achieved by defining the centers of rotation for the elbow and wrist as the midpoint between lateral/medial epicondyle and radial/ulnar styloid in the anatomical calibration procedure, similar to the functional calibration procedure [49]. Despite differences in models, the correct estimation of segment lengths has a limited impact on joint angles accuracy. Existing literature on

TABLE III: Average local rotation of VIMU with respect to the segment's anatomical or functional frame, expressed as Euler angles in degrees (ZYX order)

	Upper arm VIMU [deg]		Forearm VIMU [deg]		Hand VIMU [deg]	
-	Anatomical	Functional	Anatomical	Functional	Anatomical	Functional
Z	-1.3 $\pm$ 4.8	-0.2 $\pm$ 8.0	1.8 $\pm$ 2.2	-6.2 $\pm$ 4.0	1.3 $\pm$ 1.5	-8.8 $\pm$ 8.8
Y	22.9 $\pm$ 15.4	29.9 $\pm$ 7.5	-11.7 $\pm$ 13.6	4.2 $\pm$ 11.7	-3.6 $\pm$ 5.6	1.22 $\pm$ 3.3
X	4.3 $\pm$ 4.5	13.8 $\pm$ 4.8	-1.2 $\pm$ 3.0	7.2 $\pm$ 1.8	1.8 $\pm$ 3.3	7.3 $\pm$ 5.3

lower limb studies with skin markers supports the notion that segment length is not a highly sensitive parameter [51]–[53]. Disparities in local rotation of VIMU result from differences in segment frame rotations defined by anatomical and functional calibration procedures.

Tables I, II, III, and Fig. 6 present additional insights. The RMSE with a multi-body IK using VIMU data is below 10 deg, falling short of the 5 deg limit acknowledged for clinical applications like marker-based gait analysis [54]. This can be explained by the fact that our method uses affordable IMUs costing 15€ and affordable cameras costing 70€, compared to other literature studies that use more cameras or more expensive IMUs [21], [29], [55]. Furthermore, most methods in the literature [21], [29], [55] rely on IMUs that use magnetometers, which are very sensitive to ferromagnetic disturbances [56]. Numerous studies in the field [21], [29], [57], which employ machine learning techniques for joint angle estimation, utilize datasets [30], [31] based on reference data using marker-sets which do not conform to the standards recommended by the International Society of Biomechanics. In our research, comparisons between anatomical and functional calibration procedures indicated a difference of up to 5 degrees in joint angles when when using two different calibration methods and OMC data (see Fig. 6, and Table I). Notably, this discrepancy reduced from 5 degrees to 0.8 degrees upon the removal of joint calibration offsets, suggesting that the variation is largely attributable to differences in the definition of segments' anatomical axes. This observation underscores the potential disparities between joint angles reported in existing literature datasets and actual ground-truth joint angles.

Removing joint calibration offsets from VIMU-derived joint angles with multi-body IK decreases the RMSE to as low as 2.4 deg, underscoring the importance of the often-overlooked calibration phase when using affordable sensors such as IMUs and camera-based markerless algorithms. While joint angles with the offset removed are valuable for estimating motion amplitude and temporal features, caution is advised when absolute segment pose is required, particularly in scenarios like inverse dynamics, where the absolute segment pose in relation to the gravity vector is crucial.

Using a multi-body IK with affordable VIMU data yields superior results, with a 68% lower error rate compared to single-body IK. This aligns with literature observations, showcasing the robustness of multi-body IK against measurement outliers [3], [5], [6]. The implemented single-body IK, similar to classical ones in the literature [11], [34], [58], estimates segment rotation through angular velocity and rotation measurements. In contrast, multi-body IK estimates both segment rotations and positions, relying on fiducial marker 3D positions and IMU linear acceleration measurements. The accuracy gap between single-body IK and multi-body IK arises from the robustness of the latter to measurement outliers, driven by inherent mechanical constraints, and differences in the measurements used for each IK method. Additional measurements of fiducial marker positions and IMU linear acceleration are beneficial with precise sensor-to-segment calibration. Even minor disparities in IMU placement can significantly hinder accurate acceleration tracking.

The present study is subject to several limitations. First, it does not encompass tasks involving whole-body movements, as the participants were seated and stationary. Additionally, our methodology is based on a traditional EKF approach for multi-body IK [42], [47], without a direct comparison to newer methods, such as those employing machine learning [55], horizon-based optimization [20], [55], or a combination of optimization and machine learning [17]. Another constraint is that the experiments were conducted under optimal lighting and measurement conditions, a necessity given the limited quality of the affordable cameras and sensors used.

V. Conclusion

In summary, our analysis underscores the crucial role of calibration consistency between VIMU and reference systems, such as stereophotogrammetry, in determining joint angle estimate accuracy. The RMSE is inherently dependent on reference system data processing, emphasizing the need for identical calibration procedures for both VIMU and reference data. Consistent calibration procedures result in an RMSE as low as 7.9 deg. Overall, our findings emphasize the superiority of multi-body IK over single-body IK when utilizing affordable VIMU data for joint angle estimation. This superiority is attributed to the robustness of multi-body IK in handling measurement outliers and the additional information provided by fiducial marker 3D positions and IMU linear acceleration measurements, further highlighting its suitability for biomechanical applications. Future research should aim to validate the methodology in more varied and challenging scenarios and under less ideal conditions, with the same affordable setup.

References

[1] A. Heller, D. Wade, V. Wood, A. Sunderland, R. Hewer, E. Ward, Arm function after stroke - measurement and recovery over the 1st 3 months, Journal of neurology, neurosurgery, and psychiatry (1987).

[2] C. Lavernia, M. D'Apuzzo, M. D. Rossi, D. Lee, The Journal of Arthroplasty (2008).

[3] T.-W. Lu, J. O'Connor, Bone position estimation from skin marker coordinates using global optimisation with joint constraints, Journal of Biomechanics (1999).

[4] M. Begon, M. Andersen, R. Dumas, Multibody kinematic optimization for the estimation of upper and lower limb human joint kinematics: a systematic review, Journal of Biomechanical Engineering (2017).

[5] A. Leardini, L. Chiari, U. Della Croce, A. Cappozzo, Human movement analysis using stereophotogrammetry part 3. soft tissue artifact assessment and compensation, Gait & posture 21 (2005) 212–25. doi:10.1016/j.gaitpost.2004.05.002.

[6] S. Duprey, A. Naaim, F. Moissenet, M. Begon, L. Cheze, Kinematic models of the upper limb joints for multibody kinematic optimisation: An overview, Journal of Biomechanics (2016).

[7] R. Mallat, V. Bonnet, M. Khalil, S. Mohammed, Upper limbs kinematics estimation using affordable visual-inertial sensors, IEEE Transactions on Automation Science and Engineering (2020).

[8] L. Chen, H. Wei, J. Ferryman, A survey of human motion analysis using depth imagery, Pattern Recognition Letters (2013).

[9] D. Mehta, S. Sridhar, O. Sotnychenko, H. Rhodin, M. Shafiei Rezvani Nezhad, H.-P. Seidel, W. Xu, D. Casas, C. Theobalt, Vnect: Real-time 3d human pose estimation with a single rgb camera, ACM Transactions on Graphics (2017).

[10] R. Bashirov, A. Ianina, K. Iskakov, Y. Kononenko, V. Strizhkova, V. Lempitsky, A. Vakhitov, Real-time rgbd-based extended body pose estimation (2021).

[11] I. H. López-Nava, A. Muñoz-Meléndez, Wearable inertial sensors for human motion analysis: A review, IEEE Sensors Journal (2016).

[12] S. Feng, R. Murray-Smith, Fusing Kinect sensor and inertial sensors with multi-rate Kalman filter (2014).

[13] Y.-C. Du, C.-B. Shih, S.-C. Fan, H.-T. Lin, P.-J. Chen, An IMU-compensated skeletal tracking system using Kinect for the upper limb, Microsystem Technologies (2018).

[14] T. Li, H. Yu, Upper-body pose estimation using a visual-inertial sensor system with automatic sensorto-segment calibration, IEEE Sensors Journal (2023).

[15] J. Colombel, V. Bonnet, D. Daney, R. Dumas, A. Seilles, F. Charpillet, Physically consistent whole-body kinematics assessment based on an rgb-d sensor. application to simple rehabilitation exercises, Sensors (2020).

[16] B. Lahkar, A. Muller, R. Dumas, L. Reveret, T. Robert, Accuracy of a markerless motion capture system in estimating upper extremity kinematics during boxing, Frontiers in Sports and Active Living (2022).

[17] S. D. Uhlrich, A. Falisse, L. Kidzinski, J. Muccini, M. Ko, A. S. Chaudhari, J. L. Hicks, S. L. Delp, Opencap: Human movement dynamics from smartphone videos, PLOS Computational Biology (2023).

[18] P. Picerno, P. Caliandro, C. Iacovelli, C. Simbolotti, M. Crabolu, D. Pani, G. Vannozzi, G. Reale, P. Rossini, L. Padua, A. Cereatti, Upper limb joint kinematics using wearable magnetic and inertial measurement units: an anatomical calibration procedure based on bony landmark identification, Scientific Reports (2019).

[19] L. Meng, M. Chen, B. Li, F. He, R. Xu, D. Ming, An inertial-based upper-limb motion assessment model: Performance validation across various motion tasks, IEEE Sensors Journal (2023).

[20] M. Adjel, M. Sabbah, R. Dumas, N. Mansard, S. Mohammed, W. Bruno, V. Bonnet, Multi-modal upper limbs human motion estimation from a reduced set of affordable sensors, IEEE IROS (2023).

[21] S. Shin, Z. Li, E. Halilaj, Markerless motion tracking with noisy video and imu data, IEEE transactions on bio-medical engineering (2023).

[22] B. Bouvier, S. Duprey, L. Claudon, R. Dumas, A. Savescu, Upper limb kinematics using inertial and magnetic sensors: Comparison of sensor-to-segment calibrations, Sensors (Basel, Switzerland) (2015).

[23] X. Robert-Lachaine, H. Mecheri, C. Larue, A. Plamondon, Accuracy and repeatability of single-pose calibration of inertial measurement units for whole-body motion analysis, Gait & Posture (2017).

[24] A. Cutti, A. Giovanardi, L. Rocchi, A. Davalli, R. Sacchetti, Ambulatory measurement of shoulder and elbow kinematics through inertial and magnetic sensors, Medical & biological engineering & computing (2008).

[25] I. Weygers, M. Kok, T. Seel, D. Shah, O. Taylan, L. Scheys, H. Hallez, K. Claeys, In-vitro validation of inertial-sensor-to-bone alignment, Journal of Biomechanics 128 (2021).

[26] G. Wu, F. van der Helm, D. Veeger, M. Makhsous, P. Roy, C. Anglin, J. Nagels, A. Karduna, K. McQuade, X. Wang, F. Werner, B. Buchholz, Isb recommendation on definitions of joint coordinate systems of various joints for the reporting of human joint motion - part ii: Shoulder, elbow, wrist and hand, J. Biomechs (2005).

[27] P. Picerno, A. Cereatti, A. Cappozzo, Joint kinematics estimate using wearable inertial and magnetic sensing modules, Gait & Posture 28 (2008).

[28] M. Bisi, R. Stagni, A. Caroselli, A. Cappello, Anatomical calibration for wearable motion capture systems: Video calibrated anatomical system technique, Medical engineering & physics (2015).

[29] X. Yi, Y. Zhou, F. Xu, Transpose: Real-time 3d human translation and pose estimation with six inertial sensors, ACM Transactions on Graphics (2021).

[30] N. Mahmood, N. Ghorbani, N. F. Troje, G. Pons-Moll, M. J. Black, AMASS: Archive of motion capture as surface shapes (2019) 5442–5451.

[31] Y. Huang, M. Kaufmann, E. Aksan, M. J. Black, O. Hilliges, G. Pons-Moll, Deep inertial poser learning to reconstruct human pose from sparseinertial measurements in real time, ACM Transactions on Graphics, (Proc. SIGGRAPH Asia) (2018).

[32] V. Guzov, A. Mir, T. Sattler, G. Pons-Moll, Human poseitioning system (hps): 3d human pose estimation and self-localization in large scenes from body-mounted sensors (2021).

[33] M. Trumble, A. Gilbert, C. Malleson, A. Hilton, J. Collomosse, Total capture: 3d human pose estimation fusing video and inertial sensors (2017).

[34] M. Nazarahari, H. Rouhani, 40 years of sensor fusion for orientation tracking via magnetic and inertial measurement units: Methods, lessons learned, and future challenges, Information Fusion (2021).

[35] G. Rab, K. Petuskey, A. Bagley, A method for determination of upper extremity kinematics, Gait & posture 15 (2002).

[36] R. M. Ehrig, W. R. Taylor, G. N. Duda, M. O. Heller, A survey of formal methods for determining the centre of rotation of ball joints, Journal of Biomechanics (2006).

[37] R. Ehrig, W. R. Taylor, G. N. Duda, M. O. Heller, A survey for formal methods for determining functional joint axes, Journal of Biomechanics (2007).

[38] F. J. Romero-Ramirez, R. Muñoz-Salinas, R. Medina-Carnicer, Tracking fiducial markers with discriminative correlation filters, Image and Vision Computing 107 (2021).

[39] J. Diebel, Representing attitude : Euler angles , unit quaternions , and rotation vectors (2006).

[40] J. Carpentier, G. Saurel, G. Buondonno, J. Mirabel, F. Lamiraux, O. Stasse, N. Mansard, The pinocchio c++ library – a fast and flexible implementation of rigid body dynamics algorithms and their analytical derivatives (2019).

[41] P. Cerveri, A. Pedotti, G. Ferrigno, Robust recovery of human motion from video using kalman filters and virtual humans, Human movement science (2003).

[42] P. Cerveri, A. Pedotti, G. Ferrigno, Robust recovery of human motion from video using kalman filters and virtual humans, Human movement science (2003).

[43] R. Mallat, Toward an affordable multi-modal motion capture system framework for human kinematics and kinetics assessment, Ph.D. thesis (2021).

[44] A. Sabatini, Kalman-filter-based orientation determination using inertial/magnetic sensors: Observability analysis and performance evaluation, Sensors (Basel, Switzerland) (2011).

[45] W. HJ., 3-d attitude representation of human joints: a standardization proposal, J Biomech (1994).

[46] L. Chéze, Comparison of different calculations of three-dimensional joint kinematics from video-based system data, Journal of Biomechanics (2000).

[47] V. Fohanno, M. Begon, P. Lacouture, F. Colloud, Estimating joint kinematics of a whole body chain model with closed-loop constraints, Multibody System Dynamics (2014).

[48] I. Söderkvist, P. Åke Wedin, Determining the movements of the skeleton using well-configured markers, J. Biomechs (1993).

[49] R. Ehrig, W. Taylor, G. Duda, M. Heller, A survey of formal methods for determining the centre of rotation of ball joints, Journal of biomechanics (2006).

[50] R. Ehrig, W. Taylor, G. Duda, M. Heller, A survey of formal methods for determining functional joint axes, Journal of biomechanics (2007).

[51] J. Roeck, K. Duquesne, J. Van Houcke, E. Audenaert, Statistical-shape prediction of lower limb kinematics during cycling, squatting, lunging, and stepping—are bone geometry predictors helpful?, Frontiers in Bioengineering and Biotechnology (2021).

[52] A. El Habachi, F. Moissenet, S. Duprey, L. Cheze, R. Dumas, Global sensitivity analysis of the joint kinematics during gait to the parameters of a lower limb multi-body model, Med Biol Eng Comput (2015).

[53] E. Jacquelin, D. Brizard, R. Dumas, A screening method to analyse the sensitivity of a lower limb multibody kinematic model, Computer Methods in Biomechanics and Biomedical Engineering (2019).

[54] J. Mcginley, R. Baker, R. Wolfe, M. Morris, The reliability of three-dimensional kinematic gait measurements: A systematic review, Gait & posture (2008).
[55] O. Pearl, S. Shin, A. Godura, S. Bergbreiter, E. Halilaj, Fusion of video and imu data via dynamic optimization of a biomechanical model (2023).
[56] M. El-Gohary, J. Mcnames, Human joint angle estimation with inertial sensors and validation with a robot arm, IEEE transactions on biomedical engineering (2015).
[57] S. Shin, J. Kim, E. Halilaj, M. J. Black, Wham: Reconstructing world-grounded humans with accurate 3d motion (2023). arXiv:2312.07531.
[58] B. Bouvier, S. Duprey, L. Claudon, R. Dumas, A. Savescu, Upper limb kinematics using inertial and magnetic sensors: Comparison of sensor-to-segment calibrations, Sensors (Basel, Switzerland) (2015) 18813–33.

BIOGRAPHIES

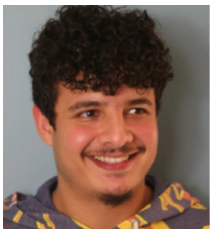

Mohamed Adjel is an engineer and M. Sc. in Industrial Engineering (and Polytech Marseille, 2020). He is currently pursuing the Ph.D. degree with the University of Paris-Est Créteil, France. His current research interests are human motion analysis, geometrical calibration and development of inverse kinematics methods from affordable sensors.

Raphael Dumas is an engineer and M. Sc. in Mechanics (INSA de Lyon, 1998), Ph.D. in Biomechanics 2002 (ENSAM de Paris, 2002), currently Senior Researcher at IFSTTAR – University of Lyon. His research interest is in three-dimensional multi-body modeling of the human musculoskeletal system applied to joint pathologies, postural and gait impairments. He is a council member of the Francophone Society of Biomechanics and Francophone Society for Movement Analysis in Child and Adult. He is regular reviewer for journals in the field of biomechanics. He has authored or co-authored 50 archive-journal full-papers, 4 book chapters and 2 patents.

Samer Mohammed (Senior Member, IEEE) received the Ph.D. degree in computer science from LIRMM/CNRS, University of Montpellier II, Montpellier, France, in 2006, and the Habilitation to supervise research degree in wearable robotics from the University of Paris-Est Créteil, Créteil, France, in 2016. He is currently a Full Professor with Université Paris-Est Créteil. He has authored or coauthored more than 100 papers in scientific journals, books, and conference proceedings. His research interests include modeling and control of robotic systems (wearable robots), artificial intelligence, and decision-support theory with target application on the functional assisting of dependent people. Dr. Mohammed is the General Chair of the IEEE-RAS Technical Committee on Wearable Robotics. He has co-organized many national and international workshops and conferences in the field of wearable technologies.

Vincent Bonnet received the Ph.D. degree in automatics control and robotics from the University of Montpellier 2, Montpellier, France, in 2009. From 2010 to 2012, he held a post-doctoral position at Foro Italico University, Rome, Italy. From 2013 to 2016, he held a post-doctoral position at the Tokyo Agricultural and Technology, Tokyo, Japan. From 2016, he held an Associate Professor position with the University of Paris Est-Créteil, Créteil, France. Since 2020, he is an Associate Professor at University of Paul Sabatier, Toulouse, France. His research interests include various aspects of low-cost sensors, motion analysis, biomechanics and movement analysis in children and adults.